Quality Tradeoffs in Object Tracking with Duty-Cycled Sensor Networks

Sadaf Zahedi and Mani B. Srivastava
Electrical Engineering Department
University of California Los angeles
Los Angeles, CA, USA
{szahedi, mbs}@ee.ucla.edu

Chatschik Bisdikian
IBM T. J. Watson Research Center
Hawthorne, NY, USA
bisdik@us.ibm.com

Lance M. Kaplan
U.S. Army Research Labratory
Adelphi, MD, USA
lance.m.kaplan@us.army.mil

Abstract—**Extending the lifetime of wireless sensor networks requires energy-conserving operations such as duty-cycling. However, such operations may impact the effectiveness of high-fidelity real-time sensing tasks, such as object tracking, which require high accuracy and short response times. In this paper, we quantify the influence of different duty-cycle schemes on the bearings-only object tracking efficiency. Specifically, we use the Maximum Likelihood localization technique to analyze the accuracy limits of object location estimates under different response latencies considering variable network density and duty-cycle parameters. Moreover, we study the tradeoffs between accuracy and response latency under various scenarios and motion patterns of the object. We have also investigated the effects of different duty-cycled schedules on the tracking accuracy using acoustic sensor data collected at Aberdeen Proving Ground, Maryland, by the U.S. Army Research Laboratory (ARL).** [1]

I. INTRODUCTION

Real-time, accurate object tracking is key to many applications such as vehicle tracking and security surveillance. Recent developments in Wireless Sensor Network (WSN) capabilities make them suitable for many applications with real-time constraints and tight deadlines on the network responses. Deadlines on the network responses to the task of interest may arise for various reasons such as the necessity for fast actions to the presence of a particular object in some strategic locations in the field. Most of the time, these networks involve a large number of sensors distributed in a vast geographical area with limited accessibility once deployed. Therefore, it is crucial to analyze and understand the expected real-time performance of WSNs before the actual deployment.

The real-time guarantee for WSN performance makes its design very challenging due to various reasons such as, (1) physical events usually have uncertain and unpredictable spatio-temporal properties which make the modeling process
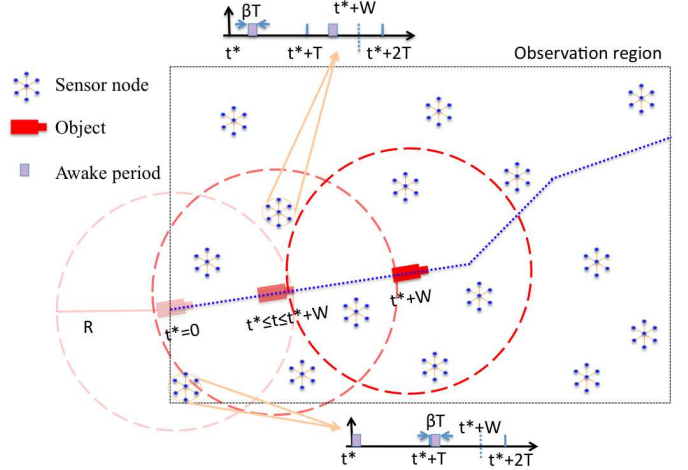
Fig. 1. Tracking scenario

hard, (2) besides the real-time responsiveness of the network, other issues such as energy efficiency and response integrity are also needed to be considered. Tracking accuracy, response latency, and energy efficiency are among the most important design metrics for tracking applications [1].

Our goal is to study the accuracy vs. response latency performance trends for an object tracking application with energy constraints. The key question of interest is: "what is the impact of different parameters of an energy saving design on the performance quality and responsiveness of the tracking task?". As an energy efficient scenario, in this work, we consider a duty-cycled network with random wake-up schedules for different sensor nodes, and focus on the delays that system may face from the duty-cycled scheme. An end-to-end delay in the network system also contains communication delay from network traffic and packet losses which are not of our focus in this work. We use both timeliness and tracking quality metrics to quantify the performance of the tracking process for each set of duty-cycle parameters. Such a multi-attribute quality consideration is in-line with Quality of Information (QoI) principles for sensor network established in [2]. The QoI metrics are highly affected by many factors including (1) object characteristics (the number

Report Documentation Page

Public reporting burden for the collection of information is estimated to average 1 hour per response, including the time for reviewing instructions, searching existing data sources, gathering and maintaining the data needed, and completing and reviewing the collection of information. Send comments regarding this burden estimate or any other aspect of this collection of information, including suggestions for reducing this burden, to Washington Headquarters Services, Directorate for Information Operations and Reports, 1215 Jefferson Davis Highway, Suite 1204, Arlington VA 22202-4302. Respondents should be aware that notwithstanding any other provision of law, no person shall be subject to a penalty for failing to comply with a collection of information if it does not display a currently valid OMB control number.

1. REPORT DATE **2010**	2. REPORT TYPE	3. DATES COVERED **00-00-2010 to 00-00-2010**

4. TITLE AND SUBTITLE **Quality Tradeoffs in Object Tracking with Duty-Cycled Sensor Networks**	5a. CONTRACT NUMBER
	5b. GRANT NUMBER
	5c. PROGRAM ELEMENT NUMBER
6. AUTHOR(S)	5d. PROJECT NUMBER
	5e. TASK NUMBER
	5f. WORK UNIT NUMBER

7. PERFORMING ORGANIZATION NAME(S) AND ADDRESS(ES) **University of California Los Angeles,Electrical Engineering Department,Los Angeles,CA,90095**	8. PERFORMING ORGANIZATION REPORT NUMBER

9. SPONSORING/MONITORING AGENCY NAME(S) AND ADDRESS(ES)	10. SPONSOR/MONITOR'S ACRONYM(S)
	11. SPONSOR/MONITOR'S REPORT NUMBER(S)

12. DISTRIBUTION/AVAILABILITY STATEMENT
Approved for public release; distribution unlimited

13. SUPPLEMENTARY NOTES
Proceedings the 31st IEEE Real-Time Systems Symposium , November-December 2010. (TR-UCLA-NESL-201008-01)

14. ABSTRACT
Extending the lifetime of wireless sensor networks requires energy-conserving operations such as duty-cycling. However such operations may impact the effectiveness of high-fidelity real-time sensing tasks, such as object tracking, which require high accuracy and short response times. In this paper, we quantify the influence of different duty-cycle schemes on the bearingsonly object tracking efficiency. Specifically, we use the Maximum Likelihood localization technique to analyze the accuracy limits of object location estimates under different response latencies considering variable network density and duty-cycle parameters. Moreover, we study the tradeoffs between accuracy and response latency under various scenarios and motion patterns of the object. We have also investigated the effects of different duty-cycled schedules on the tracking accuracy using acoustic sensor data collected at Aberdeen Proving Ground, Maryland, by the U.S. Army Research Laboratory (ARL).

15. SUBJECT TERMS

16. SECURITY CLASSIFICATION OF:			17. LIMITATION OF ABSTRACT	18. NUMBER OF PAGES	19a. NAME OF RESPONSIBLE PERSON
a. REPORT **unclassified**	b. ABSTRACT **unclassified**	c. THIS PAGE **unclassified**	**Same as Report (SAR)**	**10**	

of concurrent objects, their velocities, and moving patterns), (2) sensor characteristics (activation schedule, measurement quality, measurement type, radio range, sampling rate and transmission rate), and (3) network characteristics (topology and communication protocol).

In this work, we focus on an object tracking scenario using a network of acoustic sensor (e.g. microphone) arrays which are distributed in the observation region, see Fig. 1. At any time, the Line of Bearing (LoB) of the object vs. the sensor array center may be estimated by processing the measurements of all the sensors in one array using Minimum Variance Distortionless Response (MVDR) [3], Multi Signal Classification (MUSIC) [4], or any other similar algorithm. Having the LoB measurements of at least two sensor arrays not collinear with the object, the fusion node can process the information to localize and, ultimately, track the object(s) of interest. Bearings-only object tracking has recently raised a lot of interest in critical tracking applications [5] due to several advantages such as: (1) for an object with a smooth trajectory, the LoB does not change abruptly, which enables outlier removal from the measurements, (2) by using the MVDR or MUSIC method, circular acoustic sensor arrays with M microphones can provide information on bearing measurements of up to $M-1$ objects in the field (MUSIC requires an a priori estimate of the number of objects). This capability is a desirable feature in multi-object tracking scenarios.

Analyzing the latency and accuracy metrics for the tracking scenario of our interest is very challenging due to many reasons including the random activation schedule of the duty-cycled sensors, the unknown time of the object presence, and the uncertain object trajectory. This work is concerned in addressing the above issues. In particular, our main contributions are: (1) performance analysis of QoI attributes and their tradeoffs for bearings-only object tracking in duty-cycled WSNs using Maximum Likelihood techniques; (2) extension of the snapshot-base localization to the interval-based one and derivation of their performance bounds; and (3) computation of the probability distribution of the delay that an object tracking task may experience before the availability of enough number of applicable measurements.

The remainder of the paper is organized as follows. Section II presents the related work. Section III overviews the problem setting and our assumptions. Section IV describes the QoI analysis of bearings-only object tracking based on the Maximum Likelihood estimation techniques, and Section V discusses the simulation results. Finally Section VI concludes the paper.

II. RELATED WORK

Research on high quality tracking systems with close to real-time responsiveness has been highly investigated by the sensor network community in recent years. Various effective techniques and approaches have been proposed and verified. We here briefly review only a handful of them that are most related to this study.

The work in [6] studies the quality and energy tradeoffs for mobile object tracking by a wireless sensor network. It discusses different activation strategies including synchronized duty-cycled activation. Moreover, it is assumed that sensors are binary detectors (with classical disk model) and, at any given time, the centroid of all detecting sensors is used as an estimate for the object location. It is also shown that the duty-cycled activation offers a flexible and dynamic tradeoff between the energy expenditure and tracking error when used in conjunction with the selective activation based on the trajectory prediction. Differently from our focus in this work, authors in [6] do not analyze the effect of energy preserving schemes on the response latency and achievable tracking accuracy of the system.

The work in [1], [7], [8] presents the real-time design and analysis of VigilNet, a large-scale sensor network system which detects and classifies objects in a timely and energy efficient manner. It provides a design framework and derivations to guarantee the requested end-to-end deadline. The power management system composes of both sentry and non-sentry nodes where non-sentry nodes are sleep unless sentry nodes activate them. The sensing model and tracking algorithm are similar to those assumed in [6]. The contribution of our work compared to [1], [7], [8] is in considering the problem of bearings-only tracking and also analyzing the accuracy of tracking vs. response latency to the tracking queries. We also analyze the effect of duty-cycle parameters on the quality metrics.

In [9], using Bayesian estimation techniques, the effect of packet loss and network transport delays on the quality of object localization is studied. Sensors in [9] are always on and, hence, contrary to our work, the effect of delay due to duty-cycling is not taken into consideration. As another example of recent efforts on delay analysis for real-time detection, [10] quantifies the tradeoff between the detection delay and the false alarm rate. Besides classical disk model, a probabilistic detection model for low SNRs is used in [10] in order to analyze the minimum required network density satisfying quality performance requirements.

Next, we go over the system assumptions and problem specifications.

III. PROBLEM OVERVIEW

Throughout this work, we particularly study the tradeoffs between the response latency and the tracking accuracy of the system at times that a fusion node does not necessarily hold a high quality prior information on the object state (its recent location and velocity). This analysis is critical for many different circumstances which we mention two of them next.

The first case occurs when an object initially appears in the field, and the application has deadline requirements to receive the object location information. In this case, it is essential to analyze that how fast and with what accuracy the tracking system can track the object.

The second case happens in query-based tracking applications where the tracking system may have two different

operating phases. The first phase corresponds to the time that no query initiates from the user for that period of time. In this phase, sensor nodes may perform a low-cost local detection and report the available results to the fusion node with a moderate rate. Consequently, the fusion node exploits the global knowledge on sensor node locations and estimates the object location. The second phase starts when at time t_Q a user initiates a query like: "report the object position at time t^* by the deadline D". Receiving this query, sensor nodes switch to a higher sampling rate, perform a more advanced local processing and send their local results to the fusion node with a higher rate. Then, fusion node uses recent local information and the prior knowledge of the network to provide a high(er) quality estimate of the object location. In the case of not receiving any new measurement between t_Q and $t_Q + D$, new location is estimated based on the prior information at the fusion node.

Next, before focusing on the quality analysis, we introduce the parameters and assumptions used through the rest of the paper. As illustrated in Fig. 1, it is considered that N sensor arrays, which duty-cycle both their radios and samplers, are distributed in an observation region. They all have the same scheduling period T, and duty-cycle $\beta = \frac{\tau_{on}}{T}$ ($0 < \beta \leq 1$), where τ_{on} is the duration of "on" (awake) state. All the sensors in one array have synchronized wake-up times and are considered as one sensor node which provides LoB measurements with rate λ_s when it is on. Wake-up times for different nodes can be either selected randomly or through a systematic process. As it is shown in [1] and [8], at relatively large β (e.g., $\beta > 0.05$), the difference between the random and optimal scheduling can be practically ignored. Since the random scheduling of the wake-up times does not need any extra control message and it is not affected by time drifts, we choose a random scheduling for this work. In other words, it is assumed that different sensor nodes select their wake-up schedules independent of each other and with a uniform distribution over the cycle of T.

Fig. 2 illustrates the geometry of the object location vs. a sensor node at one snapshot. The object location and velocity at time $t \geq 0$ are $\boldsymbol{P}(t) = [P_x(t), P_y(t)]^T$ and $\boldsymbol{V}(t) = [V_x(t), V_y(t)]^T$, respectively. The ith sensor node location is $\boldsymbol{S}(i) = [S_x(i), S_y(i)]^T$, and the object state at time t is denoted by $\boldsymbol{Z}(t) = [\boldsymbol{P}(t), \boldsymbol{V}(t)]^T$. The true bearing angle $\theta_i(\boldsymbol{P}(t))$ reflects the Direction of Arrival (DoA) of the object at the time that object emitted the acoustic signal. It is assumed that the object speed is small enough such that the time retardation factor due to changes in the object location during the propagation delay is negligible. At any time t, the true bearing value from the ith sensor node is computed from

$$\theta_i(\boldsymbol{P}(t)) = \arctan\left(\frac{P_y(t) - S_y(i)}{P_x(t) - S_x(i)}\right). \tag{1}$$

The bearing measurement at time t from the ith sensor node, $\tilde{\theta}_i(t)$, $i = 1, \ldots, N$, is subject to the additive zero-mean
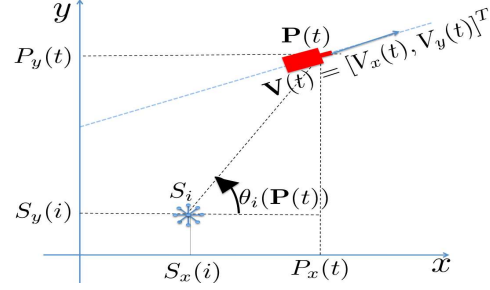

Fig. 2. Relative geometry of the object bearing line with respect to a sensor node.

Gaussian noise,

$$\tilde{\theta}_i(t) = \theta_i(\boldsymbol{P}(t)) + n_i(t), \quad n_i(t) \sim \mathcal{N}(0, \sigma_i^2). \tag{2}$$

It is assumed that sensor nodes are sufficiently separated so that the noise terms are independent. The value of bearing measurement variance σ_i^2 depends on the signal to noise ratio (SNR) of the received acoustic signal at node i and is a function of the relative distance d_i between this node and the object. In our numerical analysis, we use $\sigma_i^2 = (Kd_i^\alpha)^2$ for the bearing measurement variance [11], where K is selected such that bearing error at 1 km from the object reaches 5°. From [11] α can be chosen to be 0, 1 or 2, and we set $\alpha = 0$ in our simulations in Section V-A.

We also assume that only one object appears at any location in the observation region and its speed is low enough to allow sufficient time for awake sensor nodes to sense the object. Moreover, the object does not have any knowledge of the sensor node positions and, therefore, it can not intentionally choose a trajectory that reduces the detection probability. We furthermore use a disk model for sensing, in which a LoB of an object can be measured by a sensor node i, with measurement noise variance σ_i^2, if it is located inside a circle of radius R around the sensor node center. Using a localization algorithm, the fusion node estimates the object location based on the recent bearing measurements and available information on the object moving patterns. For the rest of the paper, we assume that the fusion node uses a Maximum Likelihood (ML) localization algorithm. The ML localization method can be used either to initially establish a track or to localize the object at any snapshot during the tracking task. Next, we describe the ML estimation techniques for both snapshot and interval-based bearings-only object tracking and analyze their quality performance.

IV. QUALITY ANALYSIS FOR BEARINGS-ONLY OBJECT TRACKING

In this section, we study the accuracy and latency quality metrics for the ML estimation using measurements of both a single snapshot and an interval. Since localization performance of an object is highly depend on the availability of the LoB measurements, we also investigate the statistics of available measurements at any snapshot and during each interval. Moreover, we analyze the distribution of a latency

that the localization task may face before having enough measurements for a well-posed tracking task.

A. Single snapshot-based tracking

As the first case, we consider a localization based on the estimated bearing measurements of one snapshot at time t. This case is useful for making fast responses to the tracking queries with short deadlines. When a query requests the object location at a later time t^* ($t^* > t_Q$), the snapshot t can be selected either very close to t^* which results in high accuracy localization, or closer to t_Q which results in a faster response to the query. For the case that $t_Q > t^*$, the snapshot t can be selected close to t_Q. In any case, for $t \neq t^*$, using the available information on the object moving patterns, the object location $\hat{P}(t^*)$ at t^* can be estimated from the computed object location at time t, $\hat{P}(t)$.

In order to have a well-posed localization problem, it is required to have LoB measurements from at least two sensor nodes non-collinear with the object. Following a query at time t_Q, due to random wake up schedules, the system may experience a delay before the object is simultaneously within the sensing range of two awake sensor nodes. The distribution of such delay is studied in Section IV-A1. Moreover, at any snapshot t, we may have different number of awake sensor nodes in the relative distance of R from the object. In this section, we first analyze the localization accuracy of a fixed number of measurements at the snapshot and then investigate the effect of randomness from wake up schedules.

Let N be the total number of sensor nodes in the range R of the object location $P(t)$. At any time t due to the randomness of wake-up schedules, we may have N_a ($0 \leq N_a \leq N$) awake sensor nodes providing N_a LoB measurements. For a feasible localization, we require to have $N_a \geq 2$ awake sensor nodes. The set of awake sensor nodes is denoted by $U = \{S_{I_1}, \ldots, S_{I_{N_a}}\}$ where indices $I_1, \ldots, I_{N_a}$ are sensor node IDs. Similar to [12] and with some notation adaptation and considering the possible non-equal measurement noise variances, from the Gaussian assumption of the measurement noise, ML localization at snapshot t can be formulated as

$$\hat{P}(t) = \arg \min_{P(t)} \sum_{k=1}^{N_a} \left(\frac{1}{\sigma_{I_k}^2} |\tilde{\theta}_{I_k} - \theta_{I_k}(P(t))|^2 \right). \quad (3)$$

In (3), $\hat{P}(t) = \{\hat{P}_x(t), \hat{P}_y(t)\}$ is the object location estimate at time t, $\tilde{\theta}_{I_k}(t)$ is the noisy bearing measurement from sensor node I_k, and $\theta_{I_k}(P(t))$ is its corresponding hypothesized bearing computed from (1). In addition, $\sigma_{I_k}^2$ is the measurement noise variance of sensor node I_k. Due to the nonlinearity of $\theta_{I_k}(P(t))$, Eq. (3) is a nonlinear Least-Squares estimator.

The ML estimator in (3) is asymptotically unbiased [13], and its error covariance is bounded below by the Cramer-Rao Lower Bound (CRLB). In addition, the covariance of ML estimator converges to CRLB when N_a goes to infinity, and for measurements with high SNR the error variance approaches the CRLB with smaller values of N_a [13].

Similar to derivations in [12], the Fisher Information Matrix (FIM) J for estimation problem (3) is

$$J = \sum_{k=1}^{N_a} \frac{1}{\sigma_{I_k}^2} \nabla \theta_{I_k} (\nabla \theta_{I_k})^T, \quad (4)$$

where $\nabla = \left[\frac{\partial}{\partial P_x(t)} \ \frac{\partial}{\partial P_y(t)} \right]^T$. Further simplification results in

$$J = \sum_{k=1}^{N_a} \left(\frac{1}{\sigma_{I_k}^2 d_{I_k}^2} A_k \right), \quad (5)$$

in which d_{I_k} is the relative distance between the object and sensor node I_k and

$$A_k = \begin{pmatrix} \sin^2(\theta_{I_k}) & -\sin(\theta_{I_k})\cos(\theta_{I_k}) \\ -\sin(\theta_{I_k})\cos(\theta_{I_k}) & \cos^2(\theta_{I_k}) \end{pmatrix}. \quad (6)$$

If C is the localization error covariance of Eq. (3), CRLB can be computed by taking inverse of J, and therefore we have $C \geqslant J^{-1}$.

Similar to [14], and with a small notation adaptation, we set the expected localization error metric

$$\rho(U) = [C]_{1,1} + [C]_{2,2}, \quad (7)$$

which is a function of the awake sensor nodes set $U = \{S_{I_1}, \ldots, S_{I_{N_a}}\}$. Here $[C]_{1,1}$ and $[C]_{2,2}$ are the first and second diagonal elements of matrix C and are the error variances in estimation of the x and y coordinates of the object. Results of Theorem 1 in [14] show that the expected position error for localization based on N_a measurements is bounded from below by

$$\rho(U) \geq 4 \left(\sum_{k=1}^{N_a} \frac{1}{\sigma_{I_k}^2 d_{I_k}^2} \right)^{-1} = \rho_L(U), \quad (8)$$

confirming that the lower bound of the error decreases as the number of N_a available measurements increases. On the other hand, the measurements from farther sensor nodes to the object or measurements with larger noise variance, have more impact on increasing the lower bound.

Next, we use the result in (8) to quantify the lower bound on the overall expected position error of (3) where, due to the randomness of wake-up schedules, the value of N_a may vary even for a fixed β. For the error analysis, we need to consider all subsets with at least two among N sensor nodes. We have $M = 2^N - N - 1$ of subsets U_i with $1 \leq i \leq M$. With the duty-cycle β, the probability of having each sensor node in "on" state is β. Therefore, the probability of having the active set U_i is

$$P(U_i, \beta) = \beta^\gamma (1 - \beta)^{N-\gamma}, \quad (9)$$

where $\gamma = |U_i|$. Considering all the possible combinations for the awake sensor nodes and their probabilities, we can conclude the following Proposition.

Proposition 4.1: If $\mathcal{U}$ refers to the set of all sensor nodes in the object range, for a network with duty-cycle β, the total expected object localization error $\rho_T(\mathcal{U}, \beta)$ satisfies

$$\rho_T(\mathcal{U}, \beta) \geq \sum_{U_i \in \mathcal{U}} P(U_i, \beta) \rho_L(U_i) = \rho_L(\mathcal{U}, \beta), \quad (10)$$
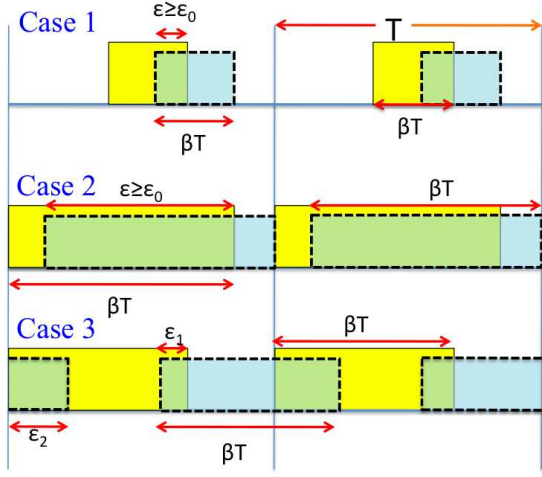
Fig. 3. Overlap between "on" states of two different sensor nodes for three different cases. Case 1 is an example of overlaps for $\epsilon_0/T < \beta \leq \frac{1}{2} + \epsilon_0/T$. Case 2 and 3 are examples of two different possible situations for $\beta > \frac{1}{2} + \epsilon_0/T$, where overlap is one segment for case 2 and two segments for case 3.

where $P(U_i, \beta)$ and $\rho_L(U_i)$ are derived from (9) and (8), respectively. In practice, due to the hardware response and sampling delay, a sensor node may experience an initial activation delay (start-up time) ϵ_0 at the beginning of its "on" state. Thus, whenever applicable, it is more precise to replace β in (9) and (10) by $\beta - \epsilon_0/T$. It is also notable that, the lower bound in (9) is particularly derived for a case that relative distances between the object and sensor nodes are known. This analysis is very useful for designers to estimate the localization error bound for strategic points in the observation region. The derivation of error lower bound for an unknown object location is the subject of our future work.

Next, in Section IV-A1, we study the delay distribution for the period of time that it takes for at least two sensor nodes in the range of the object to be awake at the same time and take measurements with negligible time differences. Moreover, in Section IV-B we extend the localization method from snapshot-based to an interval-based, which increases the chance of receiving more samples from network thus improving the tracking accuracy.

1) Delay distribution single snapshot tracking response:
To localize a moving object with no extra information on its characteristics, it is required to have (almost) synchronous LoB measurements from at least two nodes in the object range. The sensitivity level of the localization accuracy to the time difference between the samples from two different sensor nodes depends on the object speed. The faster the moving object is, the more accurate synchronization between the samples is required. Therefore, to study the delay distribution, it is necessary to investigate the probability of overlaps between "on" states of at least two of the sensor nodes in the range of the object.

Let ϵ_0 be the minimum overlap required between "on" states for a successful localization. Fig. 3 shows three examples of cases that "on" states of two sensor nodes have overlaps. For the sake of not adding an extra parameter, we assume that the object presents in an area covered by N nodes, each with a asynchronous duty-cycle β. The probability of having no intersection of equal to or greater than ϵ_0 is

$$P_{\varnothing}(N, \beta, \epsilon_0) =$$
$$\begin{cases} 1 & \beta \leq \frac{\epsilon_0}{T}, \\ \left(1 - N(\beta - \frac{\epsilon_0}{T})\right)^{N-1} & \frac{\epsilon_0}{T} < \beta < \frac{1}{N} + \frac{\epsilon_0}{T}, \\ 0 & \beta \geq \frac{1}{N} + \frac{\epsilon_0}{T}. \end{cases} \quad (11)$$

For $\beta \leq \frac{\epsilon_0}{T}$, since the maximum overlap size is βT, two sensor nodes can not have overlaps of size equal or greater than ϵ_0. For $\frac{\epsilon_0}{T} < \beta < \frac{1}{N} + \frac{\epsilon_0}{T}$, the probability is computed based on the fact that for the case of no intersection equal to or greater than ϵ_0 the distance between every two consecutive starting points of the awake states must be greater than $\beta T - \epsilon_0$. Moreover, if we fix the first starting point as the start of the cycle, the distance between the last starting point in the cycle and the end of the cycle must be greater than $\beta T - \epsilon_0$. Now that first starting point is selected, we are not allowed to put any other starting point in two intervals of size $\beta T - \epsilon_0$ at the first and end of the cycle. Therefore, all the other $N-1$ starting points have to be located in an interval of size $T - 2(\beta T - \epsilon_0)$. The minimum required distance between the start points of any two (among $N-1$) consecutive awake periods is $\beta T - \epsilon_0$. Therefore, the total minimum required distance between all consecutive pairs is $(N-2)(\beta T - \epsilon_0)$. Having that, we can uniformly distribute the start of $N-1$ awake states on the remaining interval $T - 2(\beta T - \epsilon_0) - (N-2)(\beta T - \epsilon_0)$. This will lead to the second equation in (11). Lastly, for $\beta \geq \frac{1}{N} + \frac{\epsilon_0}{T}$, there is always at least one overlap of size equal or greater than ϵ_0.

From (11), the probability of presence of at least 2 out of N sensor nodes with "on" states overlap size of equal to or greater than ϵ_0 is

$$P(N, \beta, \epsilon_0) = 1 - P_{\varnothing}(N, \beta, \epsilon_0). \quad (12)$$

It is notable that any sensor node pair with overlap of ϵ between their "on" states can be considered as a new monitoring node with a duty-cycle ϵ/T and a cycle T. The distribution of delay, t_d, of being monitored by such a node is

$$F_{t_d|\epsilon}(\tau) = P(t_d \leq \tau | \text{overlap size} = \epsilon) = \frac{\epsilon}{T} + \frac{\tau}{T}, \quad (13)$$

where $0 \leq \tau \leq T - \epsilon$. The first term in (13) refers to the case of $t_d = 0$, expressing the concurrency of the object presence (or the query time) with the overlap of the "on" states. The second term in (13) is the probability of presence of the object in the field (or receiving the query) at most τ time unit from the start of the "on" state.

Now, we use the results in (12) and (13) to approximate the delay distribution in the presence of two sensor nodes. For $\frac{\epsilon_0}{T} < \beta \leq G = \frac{1}{2} + \frac{\epsilon_0}{T}$, the size of the applicable overlaps (see an example in Fig. 3, case 1) has a uniform distribution on $[\epsilon_0, \beta T]$ with the average $\bar{\epsilon} = (\beta T + \epsilon_0)/2$. Accordingly,
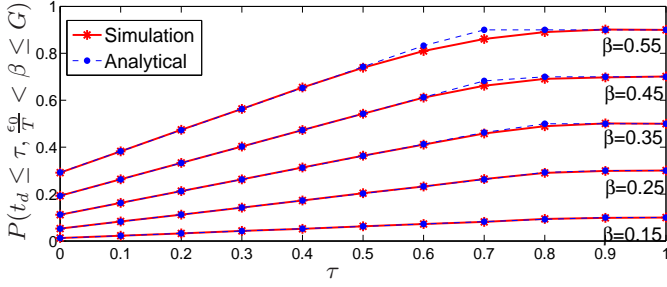
Fig. 4. Comparison of simulated and analytical results for the tracking response latency distribution at the presence of two sensor nodes. The simulated results are from a Monte Carlo simulation with a sample size 200000 for $\epsilon_0 = 0.1$, $T = 1$ and $\frac{\epsilon_0}{T} < \beta \leq G$.
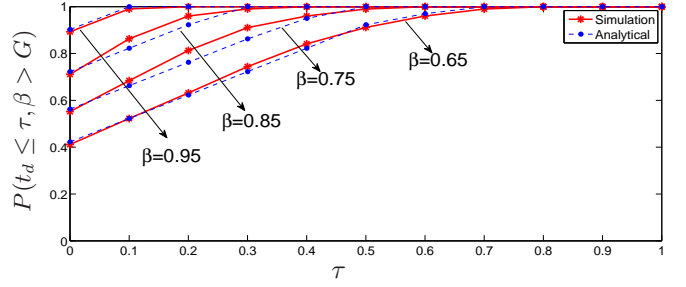

Fig. 5. Comparison of simulated and analytical results for the tracking response latency distribution at the presence of two sensor nodes. The simulated results are from a Monte Carlo simulation with a sample size 200000 for $\epsilon_0 = 0.1$, $T = 1$ and $\beta > G$.

the distribution of delay t_d is approximated by:

$$P(t_d \leq \tau, \frac{\epsilon_0}{T} < \beta \leq G) \simeq \min\left\{\frac{\bar{\epsilon}}{T} + \frac{\tau}{T}, 1\right\}(1 - P_\emptyset(2, \beta, \epsilon_0)). \quad (14)$$

The second term in (14) confirms the presence of overlaps of size equal to or greater than ϵ_0. The first term has been adopted from (13) and refers to the delay distribution for the average case with overlap size $\bar{\epsilon}$. The product of the two terms in (14) is due to the independency assumption between the detection process and the overlap occurrence. For $\beta > G$, sensor node overlaps are either one or two segments with at least one segment larger than ϵ_0. For type one (see the example in Fig. 3, case 2), the overlap size ϵ_1 is uniformly distributed on $[(2\beta - 1)T, \beta T]$ and has an average of $\bar{\epsilon}_1 = (3\beta - 1)T/2$. For type two (see an example in Fig. 3, case 3), both overlaps together have a fixed size $\epsilon_2 = 2\beta T - T$. Considering these two types of overlapping and their occurrence probabilities together with (13), the delay distribution can be approximated by

$$P(t_d \leq \tau, \beta > G) \simeq 2(1 - \beta)\min\left\{\frac{\bar{\epsilon}_1 + \tau}{T}, 1\right\} + (1 - 2(1 - \beta))\min\left\{\frac{\epsilon_2 + \tau}{T}, 1\right\}. \quad (15)$$

To verify the accuracy of the derivation in (14) and (15) we perform a Monte Carlo analysis with $\epsilon_0 = 0.1$ and $T = 1$. The outcome is reported in Figs. 4 and 5. We note that our approximate is more accurate for the case of $\frac{\epsilon_0}{T} < \beta \leq G$ compared to $\beta > G$. It is also notable that, in general, the analytical result of the distribution of the tracking for two sensor nodes can be used as an upper bound for the delay in networks with more than two sensor nodes.

In the next section, we analyze the quality of tracking with time interval measurements.

B. Interval-based tracking

As a result of duty-cycling with random schedules, for some snapshots we may not have enough awake sensor nodes in the object range. Therefore, it is beneficial to extend the localization method for single snapshot to fuse all the measurements during a time frame. In practice, the frame size

W is selected based on the application requirements and the amount of information that we have about the object. Any information on the object moving pattern such as velocity, acceleration, and also road map of the object may be used in the modeling of hypothesized bearings of different snapshots in the time frame W. With a proper selection of W, we can assume that the object velocity is constant, during each time frame, $\boldsymbol{V} = [V_x, V_y]$. We further assumed that the velocity range is such that the time retardation factor is negligible.

For the sake of simplifying the notation, in the remainder of this section, we assume that query time t_Q is the same as the time t^* that the object location requested. In this case, to localize an object at time t^*, a fusion node processes all the received sensor node measurements taken during $[t^*, t^* + W]$. Consequently, we use $N_a(W)$ to denote the number of samples received during this time frame. The ML estimator for this case is

$$\hat{\boldsymbol{Z}}(t^*) = \arg \min_{\boldsymbol{Z}(t^*)} \sum_{i=k}^{N_a(W)} \left(\frac{1}{\sigma_{I_k}^2}|\tilde{\theta}_{I_k} - \theta_{I_k}(\boldsymbol{Z}(t^*))|^2\right), \quad (16)$$

where $\hat{\boldsymbol{Z}}(t^*) = [\hat{\boldsymbol{P}}(t^*), \hat{\boldsymbol{V}}(t^*)]$ is an estimate of the location and velocity at time t^*. Indices $I_1, \ldots, I_{N_a(W)}$ in (16), refer to the sensor node IDs of all the $N_a(W)$ received measurements. Moreover, $\tilde{\theta}_{I_k}$, $1 \leq k \leq N_a(W)$, is the kth received measurement during the time frame W and $\theta_{I_k}(\boldsymbol{Z}(t^*))$ refers to the hypothesized LoB measurement. From the constant velocity assumption on the frame W, any object location at time $t \in [t^*, t^* + W]$, is given by

$$\boldsymbol{P}(t) = \boldsymbol{P}(t^*) + (t - t^*)\boldsymbol{V}(t^*). \quad (17)$$

From (17) and (1), the hypothesized LoB measurement is

$$\theta_{I_k}(\boldsymbol{Z}(t^*)) = \arctan\left(\frac{P_y(t^*) + \Delta_{I_k}V_y - S_y(I_k)}{P_x(t^*) + \Delta_{I_k}V_x - S_x(I_k)}\right). \quad (18)$$

Here $\Delta_{I_k} = t_{I_k} - t^*$ and t_{I_k} is the timestamp of the kth received measurement.

Next, we present the CRLB for the localization problem (16). Similar to the derivation in (4) and (5), the error covariance matrix can be computed from the inverse of the

FIM

$$J = \sum_{k=1}^{N_a(W)} \frac{1}{\sigma_{I_k}^2 d_{I_k}^2} \begin{pmatrix} A_{I_k} & A_{I_k}\Delta_{I_k} \\ A_{I_k}\Delta_{I_k} & A_{I_k}(\Delta_{I_k})^2 \end{pmatrix}, \quad (19)$$

where A_{I_k}, $\sigma_{I_k}^2$ and d_{I_k} are the same as in (6).

Notice that the localization performance improves with more samples $N_a(W)$ and with the smaller noise variance $\sigma_{I_k}^2$. Increasing the window size W, results in the larger $N_a(W)$ at the cost of a higher response latency and possibly the violation of the constant velocity assumption in (17). Therefore, it is important to select the proper value for W based on the application requirements and constraints. Similar to (8) and (10), we can analyze a lower bound for the localization error in (16) which is the subject of our future work.

Due to the important role of $N_a(W)$ in the localization error and the performance bound, we next study the first two statistics of $N_a(W)$ for a fixed duty-cycle. Since different sensor nodes schedule their duty-cycles independently, we can start the analysis for the case with only one sensor node in the field. Let $N_{1,a}(W)$ be the number of provided LoBs by one sensor node. Then, from the uniform distribution of the start time of the awake period over a cycle T, the average value of $N_{1,a}(W)$ is

$$E[N_{1,a}(W)] = \lfloor \beta W \lambda_s \rfloor. \quad (20)$$

Next, $Var[N_{1,a}(W)] = E[N_{1,a}^2(W)] - E[N_{1,a}(W)]^2$ is used to compute the variance value. The complete derivation of $E[N_{1,a}^2(W)]$ can be found in Appendix A, and from that the $Var[N_{1,a}(W)]$ is,

$$Var[N_{1,a}(W)] =$$
$$\begin{cases} \lambda_s^2 W^2(\beta - \frac{1}{3}\frac{W}{T} - \beta^2) & 0 < \frac{W}{T} \le \phi \\ \lambda_s^2 \phi^2(TW - \frac{1}{3}\phi T^2 - W^2) & \phi < \frac{W}{T} \le (1-\phi) \\ \lambda_s^2(T-W)^2(\beta - \frac{1}{3}\frac{T-W}{T} - \beta^2) & (1-\phi) < \frac{W}{T} \le 1 \end{cases}$$
$$(21)$$

where $\phi = \min(\beta, 1-\beta)$. Since the number of available samples in a complete cycle T is fixed, the variance has a periodic pattern. Therefore, for $W > T$, $Var[N_{1,a}(W)] = Var[N_{1,a}(w')]$ where $W \equiv w' \pmod{T}$.

Next, to compute the average and variance of available samples from all the sensor nodes in the field, we use the independency assumption between the sensor node schedules. For a network with a uniform sensor node topology of density ρ, at any time, the average number of sensor nodes in the relative distance R of the object is $\pi R^2 \rho$. Therefore, the average and variance of available number of samples from all sensor nodes in the range are

$$E[N_a(W)] = (\pi R^2 \rho)E[N_{1,a}(W)], \text{ and}$$
$$Var[N_a(W)] = (\pi R^2 \rho)^2 Var[N_{1,a}(W)]. \quad (22)$$

From (21) and (22), $Var[N_a(nT)] = 0$ for integer values of n, which results in the minimum variation for the overall localization error of (16). Also the variance value in (22) and therefore the localization performance variation are maximized for $W = nT/2$, where n is an odd integer.

In order to study the latency accuracy tradeoffs for different scenarios, in what follows, we present some test cases.

V. SIMULATION RESULTS

A. Study cases

In this section, we study the tradeoffs between the localization accuracy and its response latency through some study cases.

1) Static object and variable duty-cycle β: Similar to the illustrated scenario in Fig. 1, $N = 10$ sensor nodes are randomly deployed with a uniform distribution in an observation region of size 10×10. All the sensor nodes have the same sensing range of 8. Bearing measurements from all sensor nodes are assumed to have a zero-mean Gaussian noise with variance $\sigma^2 = 0.09$ unless specified otherwise. It is further assumed all sensor nodes duty-cycle asynchronously with the same β and T.

In this case, we have studied the performance of MLE localization in (3) for a static object. We set $t^* = 0$ as the time when the object appears in the field. At any snapshot $t \ge 0$, the fusion announces a new estimate for the object location, utilizing all the received LoBs from t^* to t. The error is defined as the Euclidean distance between the actual and estimated object location. Smaller values of the average and variance of the error imply, respectively, more accurate and less uncertain localization.

The result in Fig. 6 is computed from a Monte Carlo simulation with a sample size 4000 on the activation schedules and confirm the following points; (1) Due to the chance of receiving higher number of samples, network with a higher duty-cycle reaches a higher localization performance in a shorter time; (2) For different activation schedules, a network with a smaller duty-cycle (e.g., $\beta = 0.2$) experiences more variations in the set of awake sensor nodes. Active set variations result in different localizations and, hence, increase the variance.
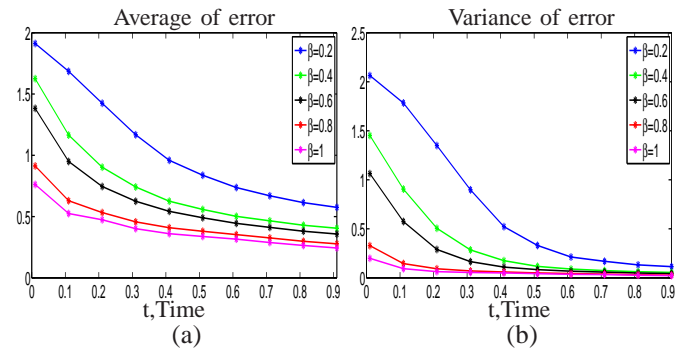

Fig. 6. (a) Average of error vs. localization response latency, (b) Variance of error vs. localization response latency for a fixed noise variance $\sigma^2 = 0.09$, $T = 1$, and different duty-cycles. The results are based on a Monte Carlo simulation with a sample size 4000 and with fixed locations for the object and sensor nodes.

2) Static object and variable noise variance σ^2: The goal of this case is to study the effect of noise variance σ^2 on the static object tracking accuracy. For this purpose, a similar scenario as in case 1 with a fixed duty-cycle $\beta = 0.5$ and three

different noise levels $\sigma^2 \in \{0.04, 0.09, 0.16\}$ is considered. As seen from Fig. 7, to guarantee a minimum localization accuracy, a system with higher noise level experiences a larger response latency.
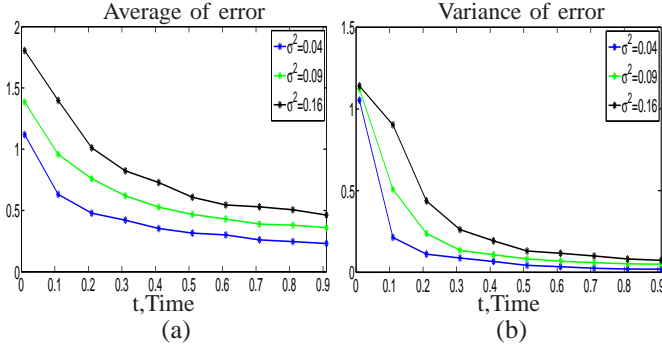

Fig. 7. (a) Average of error vs. localization response latency, (b) Variance of error vs. localization response latency for a fixed duty-cycle $\beta = 0.5$, $T = 1$, and different variances. The results are based on a Monte Carlo simulation with a sample size 4000 and fixed object and sensor node locations.

3) Static object and variable scheduling cycle T: In this case, we study the effect of schedule cycles T on the accuracy of a static object tracking. Again, a similar scenario as in Section V-A1 with a fixed duty-cycle $\beta = 0.5$ but different T values is considered. At any time instance, the parameter T does not affect the availability of each sensor node and the probability of any sensor node being awake is β. As a result, changing T does not make a difference in the snapshot-based localization. Furthermore, for an interval-based localization, to achieve the same accuracy level, networks with larger scheduling cycles experience higher latency. Results in Fig. 8 confirm the above two points at $t \simeq 0$ and $t > 0$.
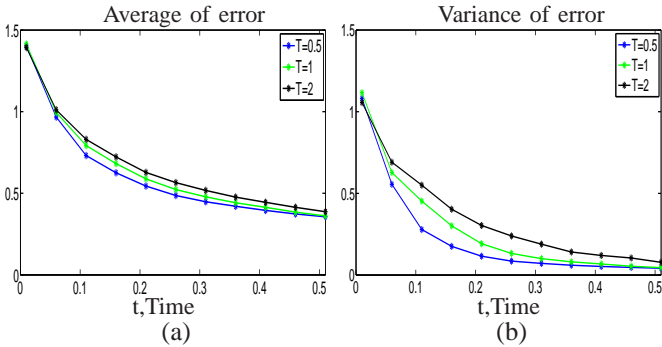

Fig. 8. (a) Average of error vs. localization response latency, (b) Variance of error vs. localization response latency for a fixed duty-cycle $\beta = 0.5$, $\sigma^2 = 0.09$, and different cycle values T. These results are based on a Monte Carlo simulation with a sample size 4000 and fixed object and sensor node locations.

4) Moving object and variable duty-cycle β: For this study, the scenario parameters are similar to those of previous cases and a moving object with constant velocity $\boldsymbol{V} = [10, -10]$ is considered. The interval-based localization approach described in Section IV-B is implemented with $W = 0.4$ and considering both conditions of known and unknown velocities. We use MLE in (16) for both conditions, where for the known velocity
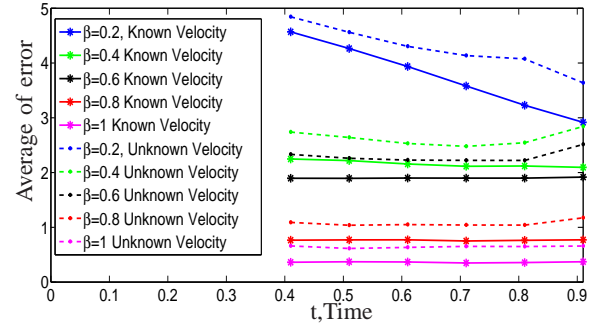

Fig. 9. Average of the interval-based localization error with $W = 0.4$ sec for a moving object and with a noise variance $\sigma^2 = 0.09$. The results are from a Monte Carlo simulation with a sample size 10000, fixed sensor node locations, and random wake-up schedules.
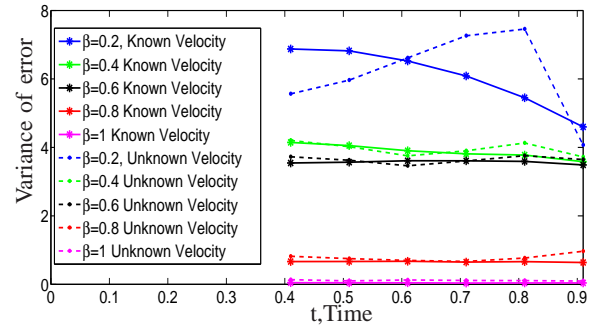

Fig. 10. Variance of of interval-based localization error with $W = 0.4$ sec for a moving object and with noise variance $\sigma^2 = 0.09$. The results are from a Monte Carlo simulation with a sample size 10000, fixed sensor node locations, and random wake-up schedules.

case, the variable $\boldsymbol{Z}_t$ is replaced by $\boldsymbol{P}_t$. The Monte Carlo simulation results under both assumptions are presented in Figs. 9 and 10. Each point with $t \geq 0.4$ sec in Fig. 9 reflects the error average of the interval-based localization over the time frame $[t - W, t]$. Similarly, Fig. 10 reflects the localization error variance. As the results in both figures confirm, higher duty-cycles β experience less localization error. Moreover, comparing error averages in Fig. 9, we experience less error when the velocity is known. Furthermore, it is notable that a network with a smaller β (e.g., $\beta = 0.2$) experiences more variations in the localization error at different times. This is a consequence of smaller $N_a(W)$ and larger sensitivity of the localization to the randomness of the awake sensor nodes set. Lastly, our localization with an unknown velocity has higher variation compared to the one with known velocity as estimating the velocity, in addition to the location, requires larger number of samples.

5) Error bound for static object with variable duty-cycle β and noise variance σ^2: In this case, we study the relationship between the expected localization error and the analytical derived lower bound in (10). A tracking scenario with parameters from Section V-A1 is considered. The error is defined as the square of the Euclidean distance and the average error is computed by a Monte Carlo simulation on
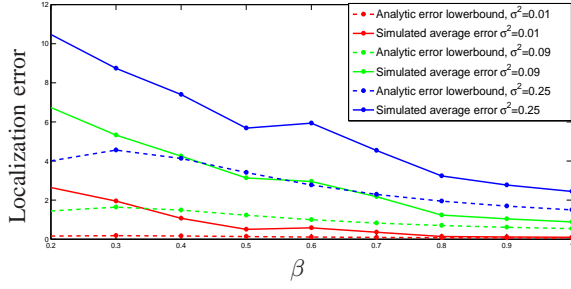
Fig. 11. Expected localization error $\rho_T(\mathcal{U}, \beta)$ vs. error lower bound $\rho_L(\mathcal{U}, \beta)$ for different bearing measurement noise variances and different β values.
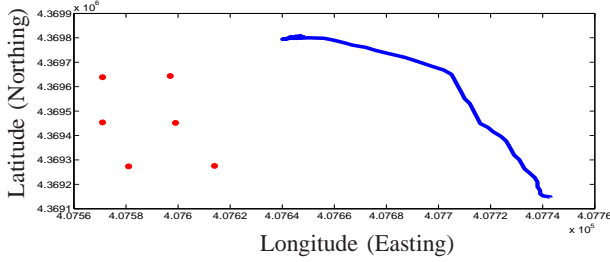

Fig. 13. (a) Average of error vs. time for $\beta = 0.5$, $T = 20$ sec, and different window sizes W. The results are from a Monte Carlo simulation with a sample size 400 on sensor node schedules.

Fig. 12. Sensor array positions and tracked vehicle trajectory in the universal transverse mercator (UTM) coordinates.

Fig. 14. Localization accuracy for $T = 20$ sec, $W = 5$ sec, and $\beta \in \{0.25, 0.5, 1\}$. The results are from a Monte Carlo simulation with a sample size 400.

the sensor node wake-up schedules. Fig. 11 shows the average error from the simulation and the analytical lower bound from (10) when different values of β and σ^2 are considered. The results in Fig. 11 confirm the following points: (1) For larger β values, a larger number of sensor nodes are awake at any snapshot resulting in a smaller localization performance variability, smaller error variance, and closer average error to its lower bound; (2) For smaller measurement noise variances σ^2, the localization accuracy is higher and the error varies less by increasing the number of measurements. Therefore, by increasing β, the average error for a smaller σ^2 has less change and is closer to the error lower bound.

B. Simulation on the real data

In this section we test the localization techniques described in Section IV on the collected data at Aberdeen Proving Ground, Maryland, by the Army Research Lab in June 2002. During the field experiment, six microphone arrays were deployed in a 2.5 Km by 2.5 Km field to collect the acoustic signature of some vehicles, see Fig. 12. The diameter of each sensor array was 8 feet and consists of 7 microphones arranged in a circular configuration. The data was collected at each sensor in the array at the rate of 1024 samples per second.

In this section, we have used the data from a period of time (60 sec) in the deployment where a tracked vehicle is traversing a path (shown in Fig. 12) from the north to south of the field. Each sensor node data is processed to obtain LoB using the MVDR method [3]. At the training phase, having the LoB measurements and exploiting the available ground truth on the vehicle trajectory, the noise level of each sensor node is estimated. To study the effect of duty-cycling
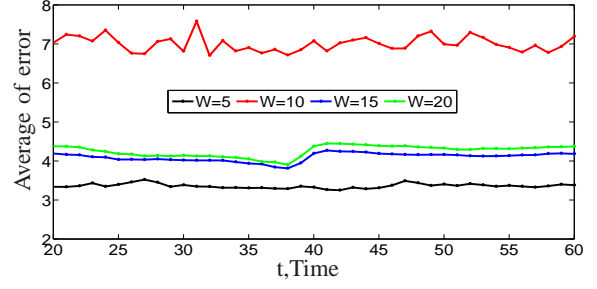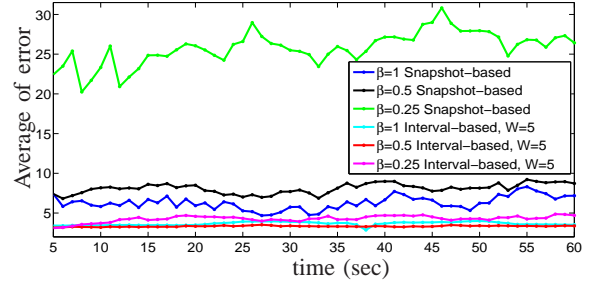
on quality metrics for tracking techniques in (3) and (16), we have selected three different duty-cycles $\beta \in \{0.25, 0.5, 1\}$ and created duty-cycled patterns with random wake-up times for all the six sensor nodes. The duty-cycle frame size T is set to 20 sec and the tracking performance for different frame sizes W is studied. Fig. 13 shows the average error for different frame size and suggests that, for this tracking problem, the interval-based tracking with $W = 5$ sec outperforms other studied time frames. Each point in Fig. 13 is the average error computed from a Monte Carlo simulation on the interval-based localization with random wake-up schedules. The error is defined as the Euclidean distance between the estimated vehicle location and its ground truth. Fig. 14 shows the average error for both snapshot and interval-based tracking for different β values. The results in Fig. 14 confirm that using higher duty-cycles and applying the interval-based localization highly improves the accuracy.

VI. CONCLUSION

In this paper, we study the effect of random duty-cycling on the accuracy and response latency of bearings-only object tracking. In order to investigate the tradeoffs between response latency and its accuracy, a set of closed-form formulas and approximations are derived. Extensive simulations are conducted to study the validity and applicability of the analysis both on the synthetic and real data. The provided analytical results in this paper are of high importance for energy efficient sensor network designs with multi-attribute Quality of Information (QoI) design metrics. Designers can apply these results to

predict the tracking performance in advance of costly deployments. Using the procedure of this work, and according to the detection requirements of the system, they can make decisions on design parameters of the system (e.g., parameters β and T for duty-cycle scheme).

To the best of our knowledge, this is the first study of its kind for object tracking that relates QoI performance metrics with duty-cycled sensor networks. It, thus, makes a significant contribution towards gaining deeper understanding of the relationship between system energy efficient parameters and achievable tracking performance.

APPENDIX A

To derive the mean of $N_{1,a}^2(W)$, we consider all possible scenarios for the overlap of an awake state of a node with the time interval $[t^*, t^* + W]$. In Fig. 15, we have selected different colors to illustrate some examples of these overlap scenarios for $W \leq T$. For simplification, and without loss of generality, we set t^* as the start of the frame ($t^* = 0$). From Fig. 15, case 1 refers to the circumstances where the interval $[t^*, t^* + W]$ either includes one complete awake state (e.g., the $\beta_1 T$ awake state in Fig. 15) or completely overlaps with an awake state (e.g., the $\beta_2 T$ awake state in Fig. 15). Case 2 refers to the situations in which the awake state partially overlaps with the interval $[t^*, t^* + W]$ and the sensor node is awake either at the start of the interval ($\beta_2 T$ example) or at the end of it ($\beta_1 T$ example). Case 3 also refers to the situations that the awake state has two overlapping segments with the interval $[t^*, t^* + W]$.

We now formulate $E[N_{1,a}^2(W)]$ with the following two assumptions: (1) To simplify the study of the statistics of $N_{1,a}^2(W)$, we approximate the analysis by replacing the non-negative discrete random variable $N_{1,a}(W)$ with a continuos random variable; (2) We neglect the effect of the sensor node start-up delay and this is justified by the assumption that the sensor node sampling rate λ_s is large enough. If we consider all the three cases in Fig. 15 and their probabilities of occurrence respectively, then $E[N_{1,a}^2(W)]$ for $0 < W \leq T$ is

$$E[N_{1,a}^2(W)] = (\alpha_1 \lambda_s)^2 \frac{|W - \beta T|}{T} + \int_{\alpha_2}^{\alpha_1} (x \lambda_s)^2 \frac{2dx}{T} + (\alpha_2 \lambda_s)^2 \frac{\alpha_2}{T}. \tag{23}$$

where $\alpha_1 = \min(\beta T, W)$ and $\alpha_2 = \max(W - (1 - \beta)T, 0)$. The first term on the right hand side of (23) corresponds to the case 1 in Fig. 15, where it considers $N_{1,a}^2(W)$ for this case multiplied by its probability. Similarly, the second and third terms in (23) refer to the case 2 and 3 in Fig. 15. Simplifying the terms in (23), $E[N_{1,a}^2(W)]$ for $0 < W \leq T$ is,

$$E[N_{1,a}^2(W)] =$$
$$\begin{cases} \lambda_s^2 W^2 (\beta - \frac{1}{3}\frac{W}{T}) & 0 < \frac{W}{T} \leq \phi \\ \lambda_s^2 \phi^2 (TW - \frac{1}{3}\phi T^2) & \phi < \frac{W}{T} \leq (1 - \phi) \\ \lambda_s^2 (X)^2 (\beta - \frac{1}{3}\frac{X}{T} - \beta^2) + \beta^2 W^2 \lambda_s^2 & (1 - \phi) < \frac{W}{T} \leq 1 \end{cases} \tag{24}$$
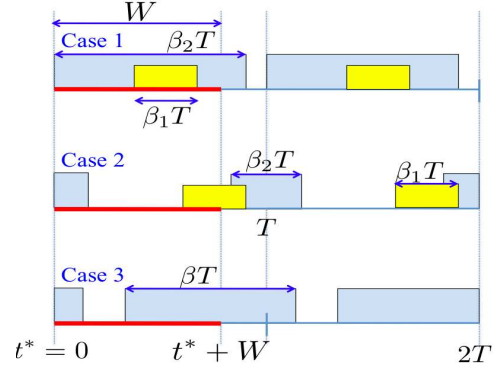

Fig. 15. Different cases of overlaps between the awake time and the monitoring interval $[t^*, t^* + W]$, where $W \leq T$.

where $\phi = \min(\beta, 1 - \beta)$, and $X = T - W$.

REFERENCES

[1] Q. Cao, T. Yan, J. Stankovic, and T. Abdelzaher, "Analysis of target detection performance for wireless sensor networks," in *DCOSS*, 2005.

[2] C. Bisdikian, L. M. Kaplan, M. B. Srivastava, D. J. Thornley, D. Verma, and R. I. Young, "Building principles for a quality of information specification for sensor information," *12th International Conference on Information Fusion*, July 2009.

[3] B. V. Veen, "Minimum variance beamforming," in *Adaptive radar detection and estimation*, 1992, p. 167.

[4] T. Pham and B. Sadler, "Wideband array processing algorithms for acoustic tracking of ground vehicles," in *21st Army Science Conference*, Norfolk, VA, June 1998.

[5] T. R. Damarla, "Tracking a convoy of multiple targets using acoustic sensor data," in *SPIE proceedings series*, 2003.

[6] S. Pattem, S. Poduri, and B. Krishnamachari, "Energy-quality tradeoffs for target tracking in wireless sensor networks," in *Second Workshop on Information Processing in Sensor Networks*, 2003.

[7] T. He, P. A. Vicaire, T. Yan, L. Luo, L. Gu, G. Zhou, R. Stoleru, Q. Cao, J. A. Stankovic, and T. Abdelzaher, "Achieving real-time target tracking using wireless sensor networks," in *TEC*, 2007.

[8] P. Vicaire, T. He, T. Yan, Q. Cao, G. Zhou, L. Gu, L. Luo, R. Stoleru, J. A. Stankovic, and T. Abdelzaherr, "Achieving long-term surveillance in vigilnet," in *ACM Transactions on Sensor Networks (TOSN)*, vol. 5, no. 9, 2009.

[9] W. Wei, T. He, C. Bisdikian, D. Goeckel, and D. Towsley, "Target tracking with packet delays and losses -qoi amid latencies and missing data," in *The Second International Workshop on Information Quality and Quality of Service for Pervasive Computing*, Mannheim, Germany, March 2010.

[10] R. Tan, G. Xing, B. Liu, and J. Wang, "Impact of data fusion on real-time detection in sensor networks," *The 30th IEEE Real-Time Systems Symposium (RTSS 2009)*, Dec 2009.

[11] Q. Le, L. M. Kaplan, and J. H. McClellan, "Kalman filtering using bearings-only measurements from a network of acoustic arrays," in *Proceedings of the ARL CTA Symposium*, College Park, MD, 2003.

[12] L. M. Kaplan and Q. Le, "On exploiting propagation delays for passive target localization using bearings-only measurements," in *Journal of Franklin Institute,*, vol. 342, 2005, p. 193211.

[13] H. Poor, *Introduction to Signal Detection and Estimation, 2nd Edition*. New York: Springer-Verlag, 1994.

[14] L. M. Kaplan, "Global node selection for localization in a distributed sensor network," in *IEEE Transactions on Aerospace and Electronic Systems*, vol. 42, no. 1, 2006, pp. 113–135.